

Role of self-assembled molecules' anchoring groups for surface defect passivation and dipole modulation in inverted perovskite solar cells

Xiaoyu Wang(王啸宇), Muhammad Faizan, Kun Zhou(周琨), Xinjiang Wang(王新江), Yuhao Fu(付钰豪), and Lijun Zhang(张立军)

Citation: Chin. Phys. B, 2024, 33 (**10**): 107303. DOI: 10.1088/1674-1056/ad711f
Journal homepage: http://cpb.iphy.ac.cn; http://iopscience.iop.org/cpb

What follows is a list of articles you may be interested in

Quantum confinement of carriers in the type-I quantum wells structure

Xinxin Li(李欣欣), Zhen Deng(邓震), Yang Jiang(江洋), Chunhua Du(杜春花), Haiqiang Jia(贾海强), Wenxin Wang(王文新), and Hong Chen(陈弘)

Chin. Phys. B, 2024, 33 (**9**): 097301. DOI: 10.1088/1674-1056/ad5d99

Topological superconductors with spin-triplet pairings and Majorana Fermi arcs

Shi Huang(黄石) and Xi Luo(罗熙)

Chin. Phys. B, 2024, 33 (**8**): 087301. DOI: 10.1088/1674-1056/ad462f

Gate-field control of valley polarization in valleytronics

Ting-Ting Zhang(张婷婷), Yilin Han(韩依琳), Run-Wu Zhang(张闰午), and Zhi-Ming Yu(余智明)

Chin. Phys. B, 2024, 33 (**6**): 067303. DOI: 10.1088/1674-1056/ad401a

Edge states enhanced by long-range hopping: An analytical study

Huiping Wang(王会平), Li Ren(任莉), Liguo Qin(秦立国), and Yueyin Qiu(邱岳寅)

Chin. Phys. B, 2021, 30 (**10**): 107301. DOI: 10.1088/1674-1056/abe9a5

Identifying anomalous Floquet edge modes via bulk-edge correspondence

Huanyu Wang(王寰宇), Wuming Liu(刘伍明)

Chin. Phys. B, 2020, 29 (**4**): 047301. DOI: 10.1088/1674-1056/ab6dcb

---

RAPID COMMUNICATION

Role of self-assembled molecules' anchoring groups for surface defect passivation and dipole modulation in inverted perovskite solar cells

Xiaoyu Wang(王啸宇)[1,†], Muhammad Faizan[2,†], Kun Zhou(周琨)[2], Xinjiang Wang(王新江)[2,‡], Yuhao Fu(付钰豪)[1,§], and Lijun Zhang(张立军)[2,¶]

[1] *Key Laboratory of Superhard Materials, College of Physics, Jilin University, Changchun* 130012, *China*
[2] *State Key Laboratory of Integrated Optoelectronics, Key Laboratory of Automobile Materials of MOE, College of Materials Science and Engineering, Jilin University, Changchun* 130012, *China*

(Received 28 July 2024; revised manuscript received 19 August 2024; accepted manuscript online 20 August 2024)

Inverted perovskite solar cells have gained prominence in industrial advancement due to their easy fabrication, low hysteresis effects, and high stability. Despite these advantages, their efficiency is currently limited by excessive defects and poor carrier transport at the perovskite–electrode interface, particularly at the buried interface between the perovskite and transparent conductive oxide (TCO). Recent efforts in the perovskite community have focused on designing novel self-assembled molecules (SAMs) to improve the quality of the buried interface. However, a notable gap remains in understanding the regulation of atomic-scale interfacial properties of SAMs between the perovskite and TCO interfaces. This understanding is crucial, particularly in terms of identifying chemically active anchoring groups. In this study, we used the star SAM ([2-(9H-carbazol-9-yl)ethyl] phosphonic acid) as the base structure to investigate the defect passivation effects of eight common anchoring groups at the perovskite–TCO interface. Our findings indicate that the phosphonic and boric acid groups exhibit notable advantages. These groups fulfill three key criteria: they provide the greatest potential for defect passivation, exhibit stable adsorption with defects, and exert significant regulatory effects on interface dipoles. Ionized anchoring groups exhibit enhanced passivation capabilities for defect energy levels due to their superior Lewis base properties, which effectively neutralize local charges near defects. Among various defect types, iodine vacancies are the easiest to passivate, whereas iodine-substituted lead defects are the most challenging to passivate. Our study provides comprehensive theoretical insights and inspiration for the design of anchoring groups in SAMs, contributing to the ongoing development of more efficient inverted perovskite solar cells.

Keywords: inverted perovskite solar cell, defect passivation, self-assembled molecule, interface engineering, first-principles calculation

PACS: 73.20.Hb, 81.65.Rv, 68.43.Bc, 31.30.jp **DOI:** 10.1088/1674-1056/ad711f

1. Introduction

The emergence of perovskite solar cells (PSCs) with inverted (p–i–n) structures holds great promise for future commercialization due to their easily scalable production, reliable performance, and improved stability.[1] In recent studies, the p–i–n PSCs and the regular (n–i–p) PSCs have achieved similar power conversion efficiencies (PCE).[2] However, for a long time, the PCE of p–i–n PSCs consistently lags behind that of their n–i–p counterparts mainly due to the low open-circuit voltage.[3] This limitation is attributed to poor interface contact quality and imperfect energy level alignment.[4] To overcome these bottlenecks, interface engineering has become a crucial way, leading to rapid improvements in the PCE of p–i–n PSCs.[5] Among all interfaces, the quality of the interface between perovskite and transparent conductive oxide (TCO), which includes materials such as fluorine tin oxide (FTO) and indium tin oxide (ITO), formed during perovskite deposition, remains the most challenging to optimize.[6] Current research focuses on achieving optimized charge transfer at the perovskite–TCO interface and controlling defects in p–i–n PSCs. In this research process, improvements in the hole transport layer materials and exploration of new materials have become focal points.[7]

In n–i–p PSCs, the most widely used hole transport materials are 2,2′,7,7′-tetrakis[N,N-di(4-methoxyphenyl)amino]-9,9′-spirobifluorene (spiro-OMeTAD) and polymer poly[bis(4-phenyl)(2,4,6-trimethylphenyl)amine] (PTAA). They offer excellent hole transport properties but are relatively expensive, posing a significant challenge to the scalability and commercial viability of PSCs.[8] Due to structural differences, the hole transport materials used in p–i–n PSCs have undergone some changes. In addition to small molecules based on triphenylamine like spiro-OMeTAD and polymers similar to PTAA, transparent inorganic materials such as NiO_x are also employed in p–i–n PSCs. While inorganic NiO_x exhibits

[†]These authors contributed equally to this work.
[‡]Corresponding author. E-mail: xinjiang_wang@jlu.edu.cn
[§]Corresponding author. E-mail: fuyuhaoy@gmail.com
[¶]Corresponding author. E-mail: lijun_zhang@jlu.edu.cn

© 2024 Chinese Physical Society and IOP Publishing Ltd

good hole transport capabilities and higher stability compared to many organic materials, its performance is still hindered by defects at the interface with perovskites.[9] Recently, self-assembled molecules (SAMs) have garnered significant attention as alternative hole transport materials.[10–12] SAMs offer distinct benefits, including minimal parasitic absorption, reduced material usage, and streamlined manufacturing processes for large-area PSCs.[13]

Typically, SAM consists of three main components: an anchoring group, a linker group, and a terminal group.[13] The special structure provides SAM with unique properties suitable for hole extraction. Taking [2-(9H-carbazol-9-yl)ethyl]phosphonic acid (2PACz) as an example, it exhibits π–π interaction between carbazoles. The π bond between carbazoles and the ability of phosphonic acid groups to anchor on substrates make 2PACz capable of forming uniform and dense monolayers. The formation of a nearly monomolecular thickness in this thin-layer form is the reason that SAMs have lower fabrication costs and reduced parasitic absorption. Meanwhile, carbazole has good conductivity and hole-extracting ability due to its conjugated nature and the donor nature.[14] of its central N atom (Fig. S1 right panel). Currently, SAMs find applications in two main ways: modifying the hole transport layer and serving directly as the hole transport layer.[15] Their low fabrication complexity and flexible, adjustable modular structure allow SAMs to effectively tune the work function of the hole transport interface and control defects. Recent research on high-efficiency p–i–n PSCs has utilized 2PACz as the hole transport layer, resulting in impressive PCEs of over 26%.[2,16,17]

In our earlier studies, we found that when SAMs are employed as a hole transport layer, they have the potential to undergo structural changes, such as flipping (Fig. 1(a)) or forming additional anisotropic layers (Fig. S1 left panel). This structural reorganization allows the anchoring group, initially intended for substrate anchoring, to interact with the perovskite, thereby achieving defect passivation.[6,18] The defect passivation capabilities facilitated by the anchoring groups of SAMs likely play a pivotal role in improving the quality of contact at the hole transport interface. However, chemical understanding of the interaction between the SAM anchoring group and perovskite surface defects is still lacking in current studies. To address this knowledge gap, we focus on modifying the anchoring group based on 2PACz in this work. We systematically evaluated the defect passivation, interface bonding stability, and interface dipole regulation of eight kinds of anchoring groups. Among all the anchoring groups, phosphonic and boric acid groups exhibit the most comprehensive interface optimization ability. This is attributed to their provision of the most diverse defect passivation configurations, the highest adsorption energies, and the most beneficial changes in interfacial dipoles. This is also confirmed by several published experimental studies.[19–24] The ionization of anchoring groups significantly enhances defect passivation ability and interface adsorption capabilities. This can be attributed to the improved Lewis base properties following ionization, which makes iodine vacancy defects in perovskite the easiest type of defect to passivate. The iodine-substituted lead defects, due to their manifestation as a Lewis base, could not be passivated in our study. Our study offers insight into the potential mechanisms underlying the optimization of the interface between perovskite and TCO using SAMs, paving the way for enhanced performance of p–i–n PSCs.

2. Computational method

We performed first-principles calculations within the framework of density-functional theory[25] using the plane-wave pseudopotential method as implemented in the Vienna *Ab initio* Simulation Package.[26,27] The electron–ion interactions were described by using the projected augmented wave pseudopotentials.[28] The $6s^26p^2$ (Pb), $5s^25p^5$ (I), $2s^22p^2$ (C), $2s^22p^3$ (N), $3s^23p^3$ (P), $2s^22p^1$(B), $3s^23p^4$ (S), $3s^23p^2$ (Si), and $2s^22p^4$ (O) were treated explicitly as valence electrons. We adopted the generalized gradient approximation formulated by Perdew, Burke, and Ernzerhof (PBE) as exchange–correlation functional.[29] To simulate the defects on the $FAPbI_3$ perovskite surfaces, we constructed $2\times2\times3$ supercells in the slab structures with a vacuum layer thickness of 15 Å. It is important to note that a supercell of this size may introduce potential defect–defect interactions. To achieve a more accurate quantitative analysis of defect charge-state transition levels, larger supercells should be constructed, and appropriate correction terms should be introduced to mitigate the errors associated with the finite supercell size. To assess the dipole regulation of SAMs on the perovskite-transparent electrode interface, we constructed an interface of $1\times1\times2$ perovskite supercell and $\sqrt{2}\times\sqrt{2}\times5$ SnO_2 supercell (simulated FTO) with [001] crystal orientation. The lattice mismatch of the interface was kept below 5%. In this study, the cubic phase $FAPbI_3$ was employed to construct the supercell. It is worth mentioning that the cubic phase, due to its dynamic instability, may induce non-physical structural relaxations in the vicinity of defects. For more precise defect analysis, it is recommended to utilize the tetragonal or orthorhombic phases, and to carefully test various crystallographic orientations during surface construction. Through partial charge density calculations, we have verified that the structural relaxations in the cubic phase do not compromise the correspondence between the Kohn–Sham defect energy levels and the point defects, thereby ensuring the validity of the qualitative analysis presented in this work. Structure optimization was achieved using the conjugate gradient technique until energies converged to 10^{-5} eV

and residual forces on atoms converged below 0.03 eV/Å. A kinetic energy cutoff of 400 eV was used for wave-function expansion, and a Monkhost *k*-mesh grid of $3 \times 3 \times 1$ was used for Brillouin zone integration. Dipole moments and electrostatic potentials of molecules after ionization were computed using the Gaussian 16 package at the B3LYP/6-311+g∗ level. The process of DFT-based calculations and analysis of the calculated results were carried out using our in-house developed code, the Jilin artificial intelligence-aided material design integrated package.[30,31]

3. Results and discussion

Based on the structure of 2PACz (Fig. 1(a) right panel), we explored common SAM anchoring group modification. In this work, we considered eight types of anchoring groups (Fig. 1(b)), including the phosphonic acid group ($–PO_3H_2$),[6] boronic acid group ($–B(OH)_2$),[32] silanetriol group ($–Si(OH)_3$),[33,34] sulfonic acid group ($–SO_3H$),[35] carboxyl group (–COOH),[36] amino group ($–NH_2$),[37] thiol group (–SH),[38] and hydroxyl group (–OH).[37] We focused exclusively on neutral point defects in perovskites. The defect energy levels were obtained by calculating the density of states (DOS). We approximated the Kohn–Sham levels within the bandgap as defect energy levels introduced by neutral defects. It should be emphasized that for a precise analysis of point defects, it is necessary to calculate the different charged states of the defects and obtain the charge-state transition levels and the corresponding defect formation energies. Considering the computational cost, we used the Kohn–Sham defect energy levels as the subject of study in this work to qualitatively investigate the passivation behavior of SAMs. Due to the high tolerance of perovskites to A-site defects,[39–41] we considered defects related to the Pb–I framework, resulting in six types: I substituted by Pb (Pb_I), Pb interstitial (Pb_i), Pb vacancy (V_{Pb}), Pb substituted by I (I_{Pb}), I interstitial (I_i), and I vacancy (V_I). Due to its relatively stable surface structure, we selected the complete octahedral surface of $FAPbI_3$ perovskite along the [001] crystal orientation. Stability tests of defect distribution in the first and second atom layers (Fig. S2) of the perovskite surface identified six specific local geometries of defects (Fig. S3). Among these defects, we found that four types of defects, namely, Pb_I, I_{Pb}, I_i, and V_I, can introduce isolated defect energy levels within the bandgap (Fig. 1(c) and S4). However, apart from the Pb_I, the other three types of defect energy levels are relatively shallow, which may not be entirely accurate since we used the semi-local PBE functional. Alkauskas *et al.* have thoroughly investigated the distribution of defect energy levels in materials such as Si, SiC, HfO_2, and SiO_2 using different functionals. They found that defect energy levels obtained with semi-local functionals tend to be relatively shallow, while those obtained with hybrid functionals are deeper.[42] Nevertheless, when using the average electrostatic potential as a reference, the two types of functionals show good agreement in describing the relative positions of different defect energy levels, indicating that semi-local functionals can accurately describe the relative positioning of defect energy levels. A similar phenomenon was observed by Ismer *et al.* in their study of point defects in AlH_3, where they found that using the PBE functional could not even yield defect energy levels within the bandgap.[43] Additionally, a review by Chen *et al.* mentioned that the accuracy of hybrid functionals in describing defect energy levels is based on their precise depiction of band edge positions and bandgaps.[44] Although the PBE functional may introduce errors in describing band edge positions, it accurately describes the bandgap of $FAPbI_3$. In summary, while the PBE functional may introduce some errors in the positioning of defect energy levels, its description of defect energy level shifts and the formation of new defect energy levels remains valuable and relevant to the core content of this study.

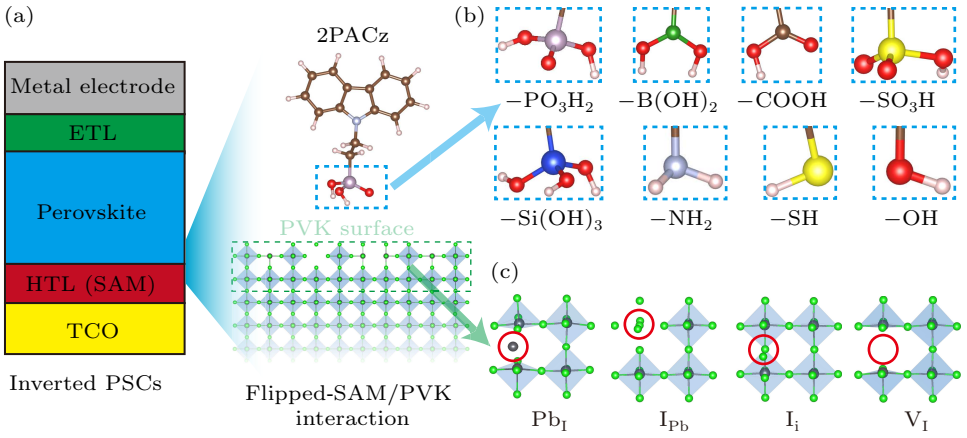


Fig. 1. (a) Schematic diagram of the structure of inverted PSCs (left panel) and the interaction between the 2PACz anchoring group and defective perovskite (PVK) surface (right panel). ETL and HTL represent electron transport layer and hole transport layer, respectively. (b) The eight anchoring groups of SAMs: phosphonic acid group ($–PO_3H_2$), boronic acid group ($–B(OH)_2$), silanetriol group ($–Si(OH)_3$), sulfonic acid group ($–SO_3H$), carboxyl group (–COOH), amino group ($–NH_2$), thiol group (–SH), hydroxyl group (–OH). (c) The optimized crystal structure of four types of point defects: I substituted by Pb (Pb_I), Pb substituted by I (I_{Pb}), I interstitial (I_i), and I vacancy (V_I).

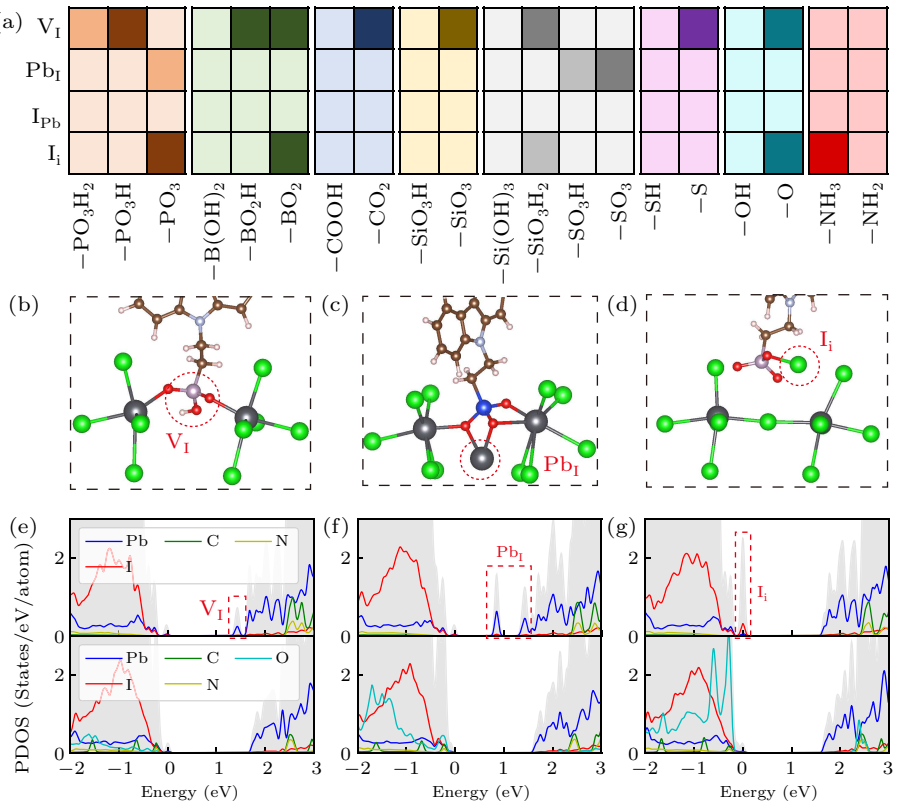


Fig. 2. (a) Statistical diagram of passivation effect of anchoring groups in different ionization states on defect energy levels in the band gap of four kinds of point defects. Color from dark to light indicates three different defect energy level passivation effects, namely, complete passivation, incomplete passivation, and no passivation effect. (b)–(d) Optimized crystal structures of three representative complete passivation cases: V_I passivated by $-PO_3H$ (b), Pb_I passivated by $-SiO_3$ (c), and I_i passivated by $-PO_3$ (d). (e)–(g) The calculated density of states for three representative cases before (upper panel) and after passivation (lower panel).

The defect energy levels introduced within the band gap by point defects on the perovskite surface are one of the primary factors leading to carrier recombination. The ability of externally introduced passivators to effectively eliminate these defect energy levels is a crucial criterion for assessing the passivation efficacy. Thiol and hydroxyl groups can undergo ionization (e.g., from $-PO_3H_2$ to $-PO_3H^-$), thereby enhancing the chemical reactivity of the anchoring group. Consequently, anchoring groups ionized to varying degrees may yield different defect passivation effects. Meanwhile, for the amine group, we only consider the protonation process ($-NH_3^+$). We introduced the anchoring groups into the A-site of the perovskite in contact with point defects to obtain the final passivation configuration through structural relaxation. Figure 2(a) illustrates the passivation effects manifested by different anchoring groups at varying degrees of ionization. The color gradient from dark to light indicates three levels of passivation effects: complete passivation, incomplete passivation, and no passivation effect. The calculated DOS corresponding to all passivation scenarios can be found in the supporting information (Figs. S5–S12). By observing the quantities under complete and incomplete passivation conditions, we determined that V_I is the most easily passivated defect, while I_{Pb} cannot be passivated by any anchoring groups. Pb_I and I_i can only be passivated in a few cases. The significant passivation effect of anchoring groups is based on the need for the oxygen in the anchoring group to bond with the undercoordinated atoms around the point defect. The donor level near the conduction band (Figs. 2(e) and 2(f)) can be removed by bonding with lead (Figs. 2(b) and 2(c)), and the acceptor level near the valence band (Fig. 2(g)) can be removed by bonding with iodine (Fig. 2(d)). Among all anchoring groups, we found that $-PO_3H_2$, $-B(OH)_2$ and $-Si(OH)_3$ have the potential to offer more than three passivation possibilities, as indicated by the dark regions in Fig. 2. Therefore, we can infer that they possess a stronger capability to passivate defects on the perovskite surface. Additionally, ionized anchoring groups demonstrate enhanced passivating capabilities. This suggests that ionized groups display high bonding activity, which increases the likelihood of inducing changes in the electronic structure of the perovskite surface.

We analyze the mechanisms of defect energy level formation and passivation from the perspective of orbital contributions. When isolated, unbonded Pb atoms appear in the perovskite lattice, they generate isolated defect energy levels within the band gap. The formation of Pb–Pb dimer results in more defect energy levels due to further orbital hybridization, lying deeper within the band gap (Fig. 3(a)). This mechanism has been observed in some earlier theoretical studies.[45,46] Disrupting the Pb–Pb dimer structure is fundamental for effec-

tively passivating deep-level defects. The active oxygen in the anchoring group bonds with Pb, which balances the charge according to the Lewis acid-base neutralization mechanism and completes the undercoordinated Pb atom. Finally, this bonding process pushes the defect state to the conduction band, effectively completing the passivation process (Fig. 3(b)). Due to the unique band edge anti-bonding electronic structure of perovskites, defect energy levels formed by excess I-atoms are generally tolerated. However, when I–I interaction occurs, they produce shallow anti-bonding states at the valence band edges (Fig. 3(c)). This defect energy level can be weakened by the formation of the O–I bond, which lowers the defect energy levels into the valence band, thus passivating the defects (Fig. 3(d)).

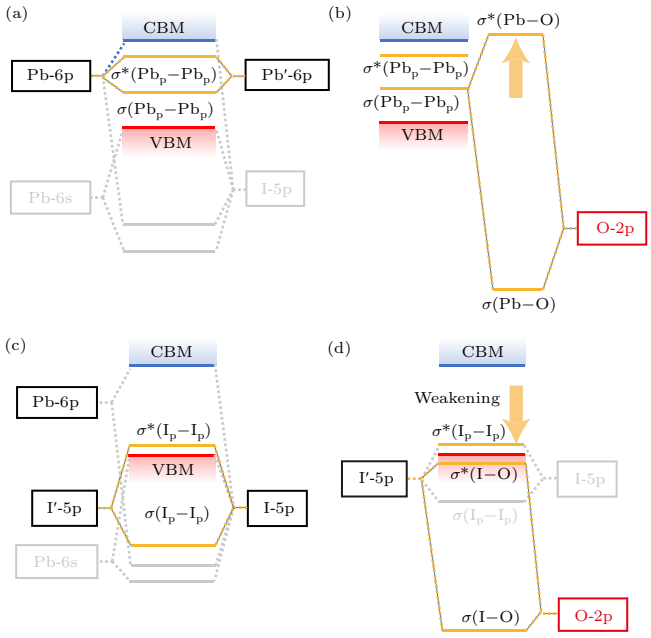


Fig. 3. (a) Schematic showing the mechanism of Pb–Pb dimmers producing multiple defect energy levels in the band gap and (b) the mechanism of eliminating defect energy levels through Pb–O bonding. (c) Diagram showing the mechanism of I–I interaction forming acceptor defect energy levels. (d) Schematic illustrating the mechanism of eliminating defect energy levels through O–I bonds.

It is worth mentioning that Lewis acid-base neutralization is the foundational process in the passivation methods discussed above. The ionized anchoring groups exhibit Lewis basicity similar to that of the original halogens (I), which enables them to effectively neutralize the lead ions adjacent to the V_I (Fig. 2(b)). This explains why the ionized anchoring groups exhibit the best passivation effects on V_I (Fig. 2(a)). A similar phenomenon of enhanced Lewis base properties leading to improved passivation capabilities was observed by Furer *et al.* in their experimental study on the modification of TCOs using Naphthalene-imide SAMs.[47] The difficulty in passivating substitution defects stems from their introduction of a stronger localized charge imbalance. Substitution defects can be approximated as complex defects comprising two types of point defects. For example, a Pb_I defect can be considered a combination of a Pb interstitial defect and an I vacancy defect. Therefore, balancing localized charges and altering the position of defect energy levels through orbital hybridization are two crucial approaches for the successful passivation of the defect energy levels.

In previous sections, we analyzed the passivation capabilities of different anchoring groups on perovskite surface defects from the perspectives of electronic structure and bonding. However, since the flipping of SAM is a rare behavior, it is also imperative to analyze the binding energies of the anchoring groups with various defects and substrate materials from a thermodynamic perspective. The calculated binding energies of anchoring groups in different ionization states with various types of defects, as well as their binding energies with the TCOs (using FTO as an example), are shown in Fig. 4. Given that we consider the ionization of anchoring groups during the adsorption process, the chemical potential of hydrogen must be considered. The formula for calculating the binding energy (E_b) of a SAM adsorbed on a specific defect on the perovskite surface is

$$\begin{aligned} E_b \;=\; & E_{\text{adsorb}}\,(\text{PVK with defect}) + n(\mu_H + \Delta\mu_H) \\ & - E_{\text{surface}}\,(\text{PVK with defect}) - E\,(\text{SAM})\,, \end{aligned} \tag{1}$$

in which E_{adsorb} (PVK with defect) represents the total energy of the perovskite with defects after adsorption of the SAM, n denotes the number of protons ionized from the SAM, E_{surface} (PVK with defect) is the energy of the perovskite surface with defects before the SAM is adsorbed. For the amine group, since it undergoes protonation ($-NH_3^+$), the value of n would be negative in this context. E (SAM) represents the energy of the SAM before ionization, μ_H is the energy of hydrogen in its elemental form (per atom), and $\Delta\mu_H$ signifies the chemical potential of hydrogen relative to its elemental form. For SAM adsorbed on an FTO surface, E_{adsorb} and E_{surface} should be replaced with the energy of the FTO surface after SAM adsorption and the energy of the FTO surface before SAM adsorption, respectively. Their binding energy can be calculated by

$$\begin{aligned} E_b \;=\; & E_{\text{adsorb}}\,(\text{FTO}) + n(\mu_H + \Delta\mu_H) \\ & - E_{\text{surface}}\,(\text{FTO}) - E\,(\text{SAM})\,. \end{aligned} \tag{2}$$

During the process of anchoring on an FTO surface, the amine group does not undergo protonation, so the value of n does not need to be negative. The range of the chemical potential of hydrogen can be determined by the thermodynamic conditions of the stability of the FA molecule, which are as follows:

$$\Delta\mu_H + \Delta\mu_C + \Delta\mu_N \geq \Delta H_f\,(\text{FA})\,, \tag{3}$$

$$\Delta\mu_H \leq 0, \tag{4}$$

$$\Delta\mu_C \leq 0, \tag{5}$$

$$\Delta\mu_N \leq 0. \tag{6}$$

The H-rich/H-poor limit is defined by $\Delta\mu_{\mathrm{H}} = 0$ and $\Delta\mu_{\mathrm{H}} = \Delta H_{\mathrm{f}}(\mathrm{FA})$. We found that all the neutral anchoring groups cannot stably adsorb on the four types of point defects, as their binding energies are all positive. Some of the ionized anchoring groups can stably adsorb defects, except $\mathrm{I_i}$ (Fig. 4(d)) under H-poor conditions. $\mathrm{Pb_I}$ is most easily adsorbed (Fig. 4(b)), followed by $\mathrm{V_I}$ (Fig. 4(a)) and $\mathrm{I_{Pb}}$ (Fig. 4(c)). Fully ionized phosphonic acid groups ($-\mathrm{PO_3^{2-}}$), boronic acid groups ($-\mathrm{BO_2^{2-}}$), and silanetriol ($-\mathrm{SiO_3^{3-}}$) have the most stable adsorption capacity, which has been validated by experimental studies. Notably, the $-\mathrm{PO_3H_2}$ group has frequently been employed as a SAM anchoring group in high-performance p–i–n[19,20] and tandem PSCs.[21,22] Although $-\mathrm{B(OH)_2}$-based SAMs are less common,[48] they have been successfully used as cross-linker dopants to enhance the stability of PSCs.[23,24] Additionally, $-\mathrm{Si(OH)_3}$ has been effectively used in n–i–p PSCs to modify the interface between the electron transport layer and the perovskite, improving perovskite films and enhancing mechanical stability.[49–51] When considering FTO, the actual chemical process of SAM anchoring on the FTO surface involves dehydration polycondensation reaction. This reaction forms a bond between the active oxygen in anchoring groups and FTO surface dangling bond. Therefore, the anchoring binding energy calculated by our model is very low. The three most stable anchoring groups for binding, $-\mathrm{PO_3H_2}$, $-\mathrm{B(OH)_2}$, and $-\mathrm{Si(OH)_3}$, are shown in Fig. 4(e).

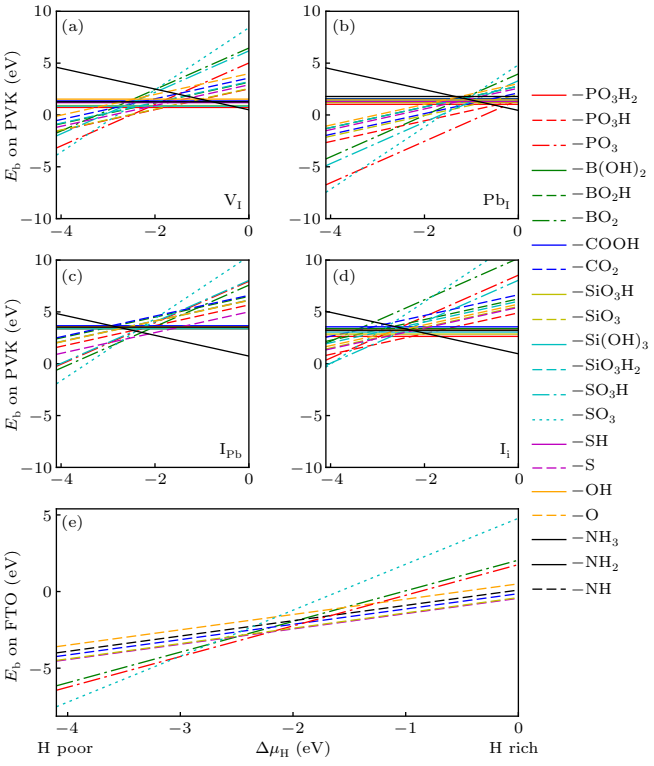


Fig. 4. Binding energies of different ionization degrees of anchoring groups with four types of defects: $\mathrm{V_I}$ (a), $\mathrm{Pb_I}$ (b), $\mathrm{I_{Pb}}$ (c), and $\mathrm{I_i}$ (d). (e) The binding energy of anchoring groups on the surface of FTO.

Although some SAMs undergo flipping and play a role in passivating point defects on the perovskite surface, their primary role remains anchored to the TCO, regulating the perovskite–TCO interface. By analyzing changes in the interfacial dipole, we can determine the specific impact of various anchoring groups on the interface hole transport. To simulate the influence of SAM on the dipole moment at the perovskite–FTO interface, we constructed a triple-layer structure of perovskite–SAM–FTO (Fig. 5). Although the molecular dipoles all point towards the carbazole group (Fig. 5(b) right panel), the dipole changes at the perovskite–FTO interface after SAMs anchored to FTO are different. Specifically, the anchoring groups $-\mathrm{PO_3H_2}$, $-\mathrm{B(OH)_2}$, and $-\mathrm{SO_3H}$ (Fig. 5(b) left panel) can introduce negative dipoles (defined as pointing from FTO to perovskite, green arrows in Fig. 5(a)). These negative dipoles facilitate the extraction of holes from the perovskite to the FTO. The $-\mathrm{PO_3H_2}$ and $-\mathrm{B(OH)_2}$ have the most significant impact on the interfacial dipole, aligning well with the calculated molecular dipoles. The sulfonic group ($-\mathrm{SO_3H}$), despite having a smaller molecular dipole, can still induce a negative dipole due to its relatively high electronegativity. On the other hand, groups with lower electronegativity, such as carboxyl, thiol, hydroxyl, and amino, may lead to a positive change in the interfacial dipole (defined as pointing from perovskite to FTO, blue arrows in Fig. 5(a)). The enhancement of hole extraction capabilities by $-\mathrm{PO_3H_2}$ and $-\mathrm{B(OH)_2}$ explains the recent experimental focus on these anchoring groups for designing high-performance hole transport SAMs.

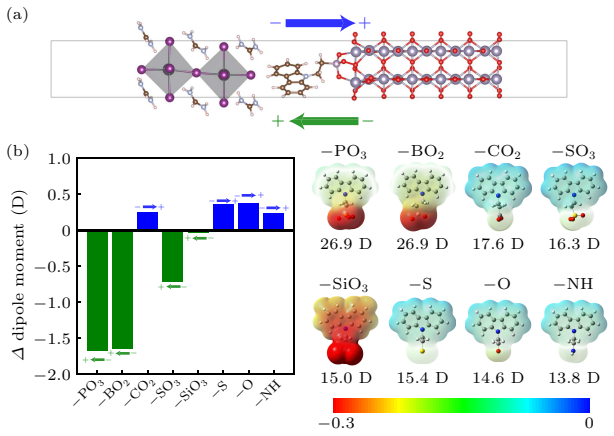


Fig. 5. (a) Schematic diagram of SAMs anchored at FTO–perovskite interface. Blue and green arrows indicate the direction in which SAMs alter the interface dipole. (b) The calculated changes in the interfacial dipole moment resulting from SAM anchoring (left panel) and the molecular dipole moment after ionization in atomic units (right panel).

4. Conclusion and outlook

Using 2PACz as the base molecule, we investigated the passivation effect of eight different anchoring groups on defects at the perovskite–TCO interface. Additionally, we studied the effects of different anchoring groups on the dipole at the perovskite–TCO interface. Passivation of defect energy

levels within the band gap is achieved by the bonding between the active oxygen in the anchoring groups and the defect atoms. Among the studied groups, $–PO_3H_2$ and $–B(OH)_2$ exhibit notable advantages in defect passivation, adsorption stability, and dipole regulation ability. They offer more passivation methods, lower adsorption energy on perovskite defects or TCOs (under H-poor conditions), and a higher degree of dipole modulation to assist in hole transport at the perovskite–TCO interface. We found that the passivation ability of anchoring groups increases significantly upon ionization. This enhancement is due to the stronger Lewis base properties of the ionized groups, which effectively neutralize the local charge environment near defects. Our results indicate that V_I defects are relatively the easiest to passivate, while defects such as Pb_I and I_{Pb}, which introduce significant charge imbalances, are more challenging to passivate. These findings are consistent with some recent studies on the design of high-performance hole transport SAMs in PSCs.

In our earlier theoretical and experimental work, we discussed the application of $–PO_3H_2$-based SAMs for modifying the flexible tandem PSCs' NiO_x layer, with a focus on the passivation of deep-level defects on the perovskite surface.[18] The concept led to the design of new SAM molecular structures, resulting in the proposal of a novel SAM and amphiphilic layered architecture, as well as the fabrication of high-efficiency p–i–n PSCs.[6] These efforts highlight the advantages of using $–PO_3H_2$ as anchoring groups in SAMs. Similarly, Kırbıyık *et al.* found that applying $–B(OH)_2$-based SAMs to modify the TiO_2 layer significantly enhances the PCE of p–i–n PSCs.[52] This demonstrates the potential applications of $–B(OH)_2$ in enhancing the efficiency and passivation of defects. Our work predicts the passivation abilities of SAM anchoring groups for perovskite surface point defects and provides valuable references for controlling the dipole at the perovskite–TCO interface. More importantly, the defect passivation approach we proposed can also be applied to the terminal group design of SAMs, enabling the creation of dual-functional SAMs that do not rely on flipping to passivate perovskite defects. In addition, we have identified favorable anchoring groups for practical applications; this demonstrates the strength of first-principles calculations in the design of SAMs. Combined with the latest machine learning technologies,[53] it is possible to accelerate the overall structure optimization of SAMs in the future, which will enhance the overall performance and efficiency of PSCs.

Acknowledgments

Project supported by the National Natural Science Foundation of China (Grant Nos. 62321166653, 22090044, and 12350410372). Calculations were performed in part at the high-performance computing center of Jilin University.

References

[1] Yao Y, Cheng C, Zhang C, Hu H, Wang K and De Wolf S 2022 *Advanced Materials* **34** 2203794
[2] Chen H, Liu C, Xu J, Maxwell A, Zhou W, Yang Y, Zhou Q, Bati A S R, Wan H, Wang Z, Zeng L, Wang J, Serles P, Liu Y, Teale S, Liu Y, Saidaminov M I, Li M, Rolston N, Hoogland S, Filleter T, Kanatzidis M G, Chen B, Ning Z and Sargent E H 2024 *Science* **384** 189
[3] Luo D, Yang W, Wang Z, Sadhanala A, Hu Q, Su R, Shivanna R, Trindade G F, Watts J F, Xu Z, Liu T, Chen K, Ye F, Wu P, Zhao L, Wu J, Tu Y, Zhang Y, Yang X, Zhang W, Friend R H, Gong Q, Snaith H J and Zhu R 2018 *Science* **360** 1442
[4] Meng L, You J, Guo T F and Yang Y 2016 *Acc. Chem. Res.* **49** 155
[5] Li M, Liu M, Qi F, Lin F R and Jen A K Y 2024 *Chem. Rev.* **124** 2138
[6] Zhang S, Ye F, Wang X, Chen R, Zhang H, Zhan L, Jiang X, Li Y, Ji X, Liu S, Yu M, Yu F, Zhang Y, Wu R, Liu Z, Ning Z, Neher D, Han L, Lin Y, Tian H, Chen W, Stolterfoht M, Zhang L, Zhu W H and Wu Y 2023 *Science* **380** 404
[7] Wang G, Chen K, Cheng L, Wang D, Meng F and Xiang W 2024 *Solar RRL* **8** 2300996
[8] Rombach F M, Haque S A and Macdonald T J 2021 *Energy Environ. Sci.* **14** 5161
[9] Park H, Chaurasiya R, Jeong B H, Sakthivel P and Park H J 2021 *Advanced Photonics Research* **2** 2000178
[10] Magomedov A, Al-Ashouri A, Kasparavičius E, Strazdaite S, Niaura G, Jošt M, Malinauskas T, Albrecht S and Getautis V 2018 *Adv. Energy Mater.* **8** 1801892
[11] Al-Ashouri A, Magomedov A, Roß M, Jošt M, Talaikis M, Chistiakova G, Bertram T, Márquez J A, Köhnen E, Kasparavičius E, Levcenco S, Gil-Escrig L, Hages C J, Schlatmann R, Rech B, Malinauskas T, Unold T, Kaufmann C A, Korte L, Niaura G, Getautis V and Albrecht S 2019 *Energy Environ. Sci.* **12** 3356
[12] Yalcin E, Can M, Rodriguez-Seco C, Aktas E, Pudi R, Cambarau W, Demic S and Palomares E 2019 *Energy Environ. Sci.* **12** 230
[13] Wang S, Guo H and Wu Y 2023 *Mater. Futures* **2** 012105
[14] Reig M, Bagdziunas G, Volyniuk D, Grazulevicius J V and Velasco D 2017 *Phys. Chem. Chem. Phys.* **19** 6721
[15] Yi Z, Li X, Xiong Y, Shen G, Zhang W, Huang Y, Jiang Q, Ng X R, Luo Y, Zheng J, Leong W L, Fu F, Bu T and Yang J 2024 *Interdisciplinary Materials* **3** 203
[16] Park S M, Wei M, Xu J, Atapattu H R, Eickemeyer F T, Darabi K, Grater L, Yang Y, Liu C, Teale S, Chen B, Chen H, Wang T, Zeng L, Maxwell A, Wang Z, Rao K R, Cai Z, Zakeeruddin S M, Pham J T, Risko C M, Amassian A, Kanatzidis M G, Graham K R, Grätzel M and Sargent E H 2023 *Science* **381** 209
[17] Li G, Su Z, Canil L, Hughes D, Aldamasy M H, Dagar J, Trofimov S, Wang L, Zuo W, Jerónimo-Rendon J J, Byranvand M M, Wang C, Zhu R, Zhang Z, Yang F, Nasti G, Naydenov B, Tsoi W C, Li Z, Gao X, Wang Z, Jia Y, Unger E, Saliba M, Li M and Abate A 2023 *Science* **379** 399
[18] Li L, Wang Y, Wang X, Lin R, Luo X, Liu Z, Zhou K, Xiong S, Bao Q, Chen G, Tian Y, Deng Y, Xiao K, Wu J, Saidaminov M I, Lin H, Ma C Q, Zhao Z, Wu Y, Zhang L and Tan H 2022 *Nat. Energy* **7** 708
[19] Park S M, Wei M, Lempesis N, Yu W, Hossain T, Agosta L, Carnevali V, Atapattu H R, Serles P, Eickemeyer F T, Shin H, Vafaie M, Choi D, Darabi K, Jung E D, Yang Y, Kim D B, Zakeeruddin S M, Chen B, Amassian A, Filleter T, Kanatzidis M G, Graham K R, Xiao L, Rothlisberger U, Grätzel M and Sargent E H 2023 *Nature* **624** 289
[20] Li Z, Sun X, Zheng X, Li B, Gao D, Zhang S, Wu X, Li S, Gong J, Luther J M, Li Z and Zhu Z 2023 *Science* **382** 284
[21] Aydin E, Ugur E, Yildirim B K, Allen T G, Dally P, Razzaq A, Cao F, Xu L, Vishal B, Yazmaciyan A, Said A A, Zhumagali S, Azmi R, Babics M, Fell A, Xiao C and De Wolf S 2023 *Nature* **623** 732
[22] Wang G, Zheng J, Duan W, Yang J, Mahmud M A, Lian Q, Tang S, Liao C, Bing J, Yi J, Leung T L, Cui X, Chen H, Jiang F, Huang Y, Lambertz A, Jankovec M, Topič M, Bremner S, Zhang Y Z, Cheng C, Ding K and Ho-Baillie A 2023 *Joule* **7** 2583
[23] Li M, Gao H, Yu L, Tang S, Peng Y, Zheng C, Xu L, Tao Y, Chen R and Huang W 2021 *Small* **17** 2102090
[24] Abbas M, Cai B, Hu J, Guo F, Mai Y and Yuan X C 2021 *ACS Appl. Mater. Interfaces* **13** 46566
[25] Hohenberg P and Kohn W 1964 *Phys. Rev.* **136** B864
[26] Kresse G and Furthmüller J 1996 *Phys. Rev. B* **54** 11169

[27] Kresse G and Furthmüller J 1996 *Computational Materials Science* **6** 15
[28] Blöchl P E 1994 *Phys. Rev. B* **50** 17953
[29] Perdew J P, Burke K and Ernzerhof M 1996 *Phys. Rev. Lett.* **77** 3865
[30] Zhao X G, Zhou K, Xing B, Zhao R, Luo S, Li T, Sun Y, Na G, Xie J, Yang X, Wang X, Wang X, He X, Lv J, Fu Y and Zhang L 2021 *Science Bulletin* **66** 1973
[31] Luo S, Xing B, Faizan M, Xie J, Zhou K, Zhao R, Li T, Wang X, Fu Y, He X, Lv J and Zhang L 2022 *J. Phys. Chem. A* **126** 4300
[32] Kırbıyık Ç, Akın Kara D, Kara K, Büyükçelebi S, Yiğit M Z, Can M and Kuş M 2019 *Applied Surface Science* **479** 177
[33] Wirth M J, Fairbank R W P and Fatunmbi H O 1997 *Science* **275** 44
[34] Singh S, Abdur R, Nam H S, Kim J H, Lee S M, Lee H and Lee J 2023 *Electron. Mater. Lett.* **19** 267
[35] Yee C, Kataby G, Ulman A, Prozorov T, White H, King A, Rafailovich M, Sokolov J and Gedanken A 1999 *Langmuir* **15** 7111
[36] Laibinis P E, Hickman J J, Wrighton M S and Whitesides G M 1989 *Science* **245** 845
[37] Chen Y, Li B, Zhong W, Luo D, Li G, Zhou C, Lan L and Chen R 2022 *IEEE Transactions on Electron Devices* **69** 160
[38] Vericat C, Vela M E, Benitez G, Carro P and Salvarezza R C 2010 *Chem. Soc. Rev.* **39** 1805
[39] Liu N and Yam C 2018 *Physical Chemistry Chemical Physics* **20** 6800
[40] Oner S M, Sezen E, Yordanli M S, Karakoc E, Deger C and Yavuz I 2022 *J. Phys. Chem. Lett.* **13** 324
[41] Yin W J, Shi T and Yan Y 2014 *Appl. Phys. Lett.* **104** 063903
[42] Alkauskas A, Broqvist P and Pasquarello A 2011 *Physica Status Solidi (b)* **248** 775
[43] Ismer L, Janotti A and Van de Walle C G 2011 *J. Alloy. Compd.* **509** S658
[44] Chen W and Pasquarello A 2015 *J. Phys.: Condens. Matter* **27** 133202
[45] Godding J S W, Ramadan A J, Lin Y H, Schutt K, Snaith H J and Wenger B 2019 *Joule* **3** 2716
[46] Fei C, Li N, Wang M, Wang X, Gu H, Chen B, Zhang Z, Ni Z, Jiao H, Xu W, Shi Z, Yan Y and Huang J 2023 *Science* **380** 823
[47] Fürer S O, Rietwyk K J, Pulvirenti F, McMeekin D P, Surmiak M A, Raga S R, Mao W, Lin X, Hora Y, Wang J, Shi Y, Barlow S, Ginger D S, Marder S R and Bach U 2023 *ACS Appl. Energy Mater.* **6** 667
[48] Guo H, Liu C, Hu H, Zhang S, Ji X, Cao X M, Ning Z, Zhu W H, Tian H and Wu Y 2023 *National Science Review* **10** nwad057
[49] Shi Y, Zhang H, Tong X, Hou X, Li F, Du Y, Wang S, Zhang Q, Liu P and Zhao X 2021 *Solar RRL* **5** 2100128
[50] Dai Z, Yadavalli S K, Chen M, Abbaspourtamijani A, Qi Y and Padture N P 2021 *Science* **372** 618
[51] Lu H, Zhuang J, Ma Z, Deng Y, Wang Q, Guo Z, Zhao S and Li H 2019 *Materials Science in Semiconductor Processing* **97** 21
[52] Kırbıyık Ç, Can M and Kuş M 2020 *Materials Science in Semiconductor Processing* **107** 104860
[53] Xu J, Chen H, Grater L, Liu C, Yang Y, Teale S, Maxwell A, Mahesh S, Wan H, Chang Y, Chen B, Rehl B, Park S M, Kanatzidis M G and Sargent E H 2023 *Nat. Mater.* **22** 1507